Self-Disciplined Large Signal Stabilizer Design for Hybrid Energy Storage System in Renewable DC Power Systems

Pengfeng Lin, *Student Member, IEEE,* Wentao Jiang, *Member, IEEE,* Pengfei Tu, *Member, IEEE,* Chi Jin, Chuanlin Zhang, *Member, IEEE,* Peng Wang, *Fellow, IEEE,*

***Abstract*—Due to the different characteristics of energy storages (ESs), proper dynamic power allocation to ESs in a hybrid energy storage system (HESS) is of high significance. To this end, integral droop (ID) controllers have been applied to a class of ESs (denoted as ES_Hs) with high ramp rates but low energy density. Conventional V-P droops have been adopted to regulate a class of ESs (referred to as ES_Ls) with high energy density but limited response speeds. Based on the cooperation of IDs and V-P droops, high/low frequency components of the load change can be autonomously responded to by ES_Hs/ES_Ls, thus possibly prolonging the HESS lifetime. However, existing works only focus on the small signal stabilization of HESSs, whose validity may only hold under certain equilibria. To address this issue, an original self-disciplined large signal stabilizing scheme is presented in this paper. Under this scheme, a compound stabilizer comprising disturbance observers and a backstepping controller is delicately designed for an ES-interfaced converter. The observers estimate the possible disturbances induced in the converter. Those estimations would be further neutralized by the backstepping controller, which simultaneously guarantees converter system stability in the large signal sense and drives the converter terminal voltage tracking the reference given by either the ID or V-P droop. Because of the proposed stabilizer, no communication happens in HESS, and the large signal stability of overall system can be spontaneously realized with rigorous mathematical proofs by Lyapunov techniques. This stabilizing scheme for HESS application is arguably reported for the first time in this paper. A detailed parameter selection guideline is also provided. The effectiveness and feasibility of the compound stabilizer are verified by both simulations and hardware experiments.**

***Index Terms*—Hybrid energy storage system, compound stabilizer, self-disciplined large signal stability, renewable DC microgrids.**

I. Introduction

Modern electrical systems have migrated from central power generation stations, transmission lines and distribution networks to businesses/households that incorporate data centers, LED lights, motor drives and electronic loads. Nearly all this equipment need a direct current (DC) power supply. Many sources, such as batteries, supercapacitors (SCs), fuel cells and PV panels, are also DC compatible. Together with the fact that DC microgrids (MGs) outperform AC ones by featuring fewer conversion stages, higher efficiency and more flexible operation, among other favorable properties, DC systems are gaining popularity and have attracted ubiquitous academic and industrial interests [1].

For DC systems with a high share of clean generation, PVs, wind turbines and other renewable energy sources (RESs) would be working at their maximum power points. These RESs simply inject power into the MG and would not participate in DC bus voltage regulation. The DC bus can actually be controlled by energy storages (ESs) that could buffer the RES powers and maintain the bus voltage at a desirable level. Although voltage regulation can also be achieved by fossil fuel sources such as microturbines and diesel generators, they are precluded from the DC MG as the intention is to investigate the adaptability of ESs to various RES and load fluctuations. As in [2], it is understood that no single ES could currently fulfill the requirements of high power density and high energy density. ESs relying on internal chemical reactions, such as lead acid batteries, may have sufficient energy densities but slow dynamic responses, and these ESs are denoted as ES_Ls for ease of explanation. Those ESs with high ramp rates but limited energy densities, such as SCs, are accordingly referred as ES_Hs. In this context, hybrid energy storage systems (HESSs) that include ESs with complementary dynamics should be constructed [3], [4].

Numerous control strategies for coordinating ESs in a HESS have been studied in the literature. The model predictive control (MPC) reported in [5] is executed in a central controller that transmits high-frequency and low-frequency power references to both ES_Ls and ES_Hs. A similar approach is reported in [6], wherein HESS economical operations are realized by sending dispatch commands from a PLC (programmable logic controller)-based control desk to individual ESs. The optimal orchestration of ES_L and ES_H is examined in [7], and a deadbeat method is proposed to generate converter duty cycles in a fully centralized way. In addition to centralized controls, power managements for HESS based on distributed communication have also been widely scrutinized. In [8], distributed controllers with multiple consensus variables directly produce current references for batteries and SCs. But the HESS is independent of droop controls and may undergo a system crash if communication links are damaged. A distributed framework is demonstrated in [9] to minimize DC bus voltage deviation and ensure accurate power sharing among ESs. The control objectives in [9] are subsequently accomplished in [10], where a hybrid discrete-continuous consensus is stated to potentially alleviate communication burdens. However, the above centralized and distributed controls, which hinge on data exchange infrastructures are extensively criticized exposed to single point of failures, which means that a failure in part of the system may stop the entire system from functioning normally. Therefore, it is preferred that the HESS can be controlled under a decentralized mechanism where no communication will be incurred. For example, a battery and an SC are separately assigned with a low-pass filter (LPF) and a high-pass filter (HPF) for apposite transient power allocation [11]. An LPF is used to filter the feedback voltage to purposely slow down battery dynamic responses [3], while other ESs will automatically handle the residual demanded power. In [2], an integral droop (ID) for ES_H is proposed to cooperate with the conventional V-P droop to naturally formulate the LPF/HPF. Then, ES_Hs and ES_Ls will automatically compensate the high- and low-frequency components of load power. Compared with the centralized and distributed schemes, the decentralized ones feature higher reliability and scalability [12].

It is imperative to point out that the correct realizations of

centralized, distributed and decentralized schemes would always necessitate stable operations at both the converter and system levels. System stability would be impaired by the destabilizing effects of constant power loads (CPLs), which normally refer to electronic loads consuming power regardless of DC bus voltage deviations. Moreover, uncertainties in system parameters and intermittencies brought about by RESs would also threaten MG stabilities. To tackle these difficulties, heterogeneous stabilization techniques have been proposed and implemented in different applications. In [13], virtual resistances are integrated at the output terminal of DC/DC converters to increase system damping. An LPF-enabled adaptive stabilizer is presented to revise droop equations in [14] to suppress resonances in close-loop transfer functions. Virtual inductors are suggested by [15] and [16] to modify converter output impedances aimed at forcing dominant poles to enter more stable regions. A conclusion opposite to those of [15] and [16] is drawn in [17], where a negative virtual inductance is proposed to offset the line inductor, thus eliminating unstable poles. The passivity-based control (PBC) documented in [18] is billed as self-disciplined stabilization such that as long as each converter in DC MG adheres to the passivity rule, then the overall system stabilization can be obtained naturally. Following [18], the effects of voltage references, input voltages and output currents on system passivity are all examined in [19]. In [20], MG passivity is further improved by inserting disturbance observers into the converter controllers. In [21], [22], decentralized controllers are proposed but they are rather complex for real engineering and may not be fit for HESSs.

Although the preceding methods are straightforward and easy to implement, they unexceptionally rely on small signal models that linearize the MG at a certain equilibrium. The analyzed results would not be valid in the presence of large load changes and considerable parameter variations. In addition, those HESS studies merely focus on ES power management which takes for granted that ES-interfaced converters are stable. They rarely touch on the issue of accomplishing HESS large signal stabilization, which would allow for a much wider operating range than that in the small signal sense [23], [24]. To fill this gap and inherit the self-disciplined stabilization concept from [18], a decentralized compound stabilizer is presented in this paper. The stabilizer is synthesized by nonlinear disturbance observers and a recursive backstepping controller [25]. Regardless of whether it is ES_L or ES_H, the interfacing DC/DC converter is uniformly equipped with compound stabilizers. For a given converter system, its power interactions with circumambient converters and interior parameter uncertainties are first estimated by the observer. The estimations are then compensated in feedforward ways by the backstepping control law, which also strictly stabilizes the converter states in the large signal sense. In this regard, the individual converter system with its ES is subject to strict stabilization that is independent of states in other electrical units. In the case that multiple ESs gather to build up a HESS, despite CPL and RES fluctuations, the large signal stabilization of the entire DC system could be autonomously achieved. This mechanism is termed self-disciplined large signal stability in this paper. The novelties of the mechanism are summarized as follows.

1) To regulate the DC bus voltage, as long as the internal ES-interfaced converters of the HESS are regulated by the compound stabilizer, then global DC system stabilization can be autonomously guaranteed. The stabilizer is realized in a fully decentralized manner, which permits flexible system expansion and plug and play (PnP) operations.

2) Different from small signal stabilizations, the validity of the proposed large signal stabilizer is not constrained to particular equilibria but instead applies to a wide range system operations. As such, it is possible to schedule the HESS to work at any point where the currents or voltages of hardware do not stretch beyond the hardware tolerable levels. Moreover, compared with PBC in [18]–[20] and the impedance-based stability analyses in [26], where the models of all power devices must be known, the compound stabilizers are only installed in the bus voltage regulating units, i.e., ESs in this paper, which makes the stabilizer much easier to implement in practical engineering. [C 1.1] By means of impedance stability criterion, in subsequent context, it will also theoretically reveal the HESS instability mechanism when the HESS is with conventional PI controls.

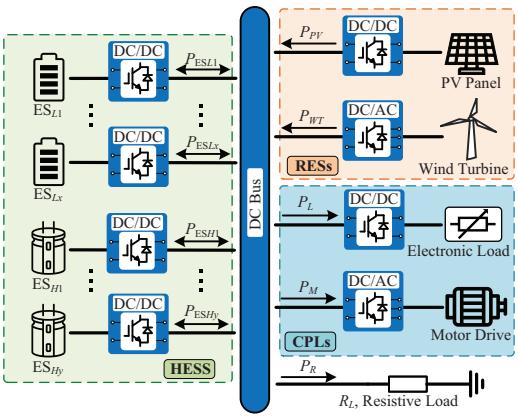

Fig. 1. A typical DC MG with a HESS, RESs and CPLs.

3) ES_L and ES_H are controlled with V-P droop and ID, respectively. The two droops convey voltage references to the proposed stabilizers, which subsequently drive the converter output voltages to track the corresponding references, without impacting the self-disciplined large signal stability of the DC system. With the coexistence of the V-P droop and ID, ES_H will spontaneously respond to the high-frequency parts of load power changes, and ES_L will slowly output the power to take up the low-frequency ones. In this way, dynamic power allocation of ES_Ls and ES_Hs in the transient state can be properly realized.

The remainder of this paper is organized as follows. Section II illustrates typical DC MG and HESS configurations. Dynamic power allocation among ES_Ls and ES_Hs will be expounded, and it is shown that commonly-used DC/DC converters can be modeled in a canonical form. Section III elucidates the step-by-step design of the compound stabilizer in a recursive framework. Self-disciplined large signal stability analyses are provided in Section IV. Sections V and VI demonstrate the simulations and experimental results. The conclusions are finally drawn in Section VII.

II. Problem Formulation

Fig. 1 illustrates a typical DC power system with a HESS, RESs and CPLs. There are x ES_Ls and y ES_Hs. P_{PV} and P_{WT} stand for the maximum RES powers that are extracted from the PV panel and wind turbine. A resistive load is directly coupled to the DC bus without any electronic device, and its power is P_R. The electronic load and motor drive can be considered as CPLs, as their absorbed powers are generally invariant for certain time durations. When RES powers exceed the power consumed by the CPLs and resistor load, the surplus power should be stored in the HESS. Otherwise, the HESS has to provide power to loads to balance the generations and consumptions in DC MG. From

the perspective of the HESS, its equivalent load can be written as follows,

$$P_{eq} = P_L + P_M + P_R - P_{PV} - P_{WT}. \quad (1)$$

A. Dynamic Power Allocation in HESSs

As explained in the Introduction, ES$_L$s are characterized by comparatively high energy density but slow dynamics, and ES$_H$s are complementary to ES$_L$s in electrical performance. It is hence desired that, in the case of P_{eq} changes, ES$_H$s can handle the surging parts in P_{eq}, and ES$_L$s can shoulder the responsibility of compensating the slow fluctuations of P_{eq}. To this end, ES$_L$s and ES$_H$s are respectively assigned V-P droops and IDs, which are detailed as follows:

$$V = V_n - m_i P_{ESLi},\ i = 1,\ 2,\ \cdots x, \quad (2)$$

$$V = V_n - n_i \frac{P_{ESHi}}{s},\ i = 1,\ 2,\ \cdots y, \quad (3)$$

where P_{ESLi} and P_{ESHi} represent powers of the ith ES$_L$ and the ith ES$_H$. m_i and n_i are the coefficients in V-P droops and IDs, respectively. V_n and V are the nominal voltage and the bus voltage in the DC power system. Then, there are three types of power sharing patterns when probing the coordination of (2) and (3), and these three patterns are carefully explained below:

1) Power sharing between the ES$_L$ cluster and ES$_H$ cluster.

As comprehended from [27], x droop formulas in (2) can be properly merged into an equivalent one,

$$V = V_n - mP_{ESL},\ m = (m_1^{-1} + m_2^{-1} + \cdots + m_x^{-1})^{-1}, \quad (4)$$

where m denotes the combined droop coefficient and $P_{ESL} = \sum_{i=1}^{x} P_{ESL}$ is the summed power of ES$_L$s. It should be noted that droop schemes are actually inherited from the frequency regulation of large-scale power systems. For a storage controlled by a V-P droop, its terminal voltage drops when its output power increases. To ensure that the bus voltage is within the proper range, m must be computed as $\Delta V_{\max}/P_{ESL\max}$, where $\Delta V_{\max}$ is the allowable maximum voltage deviation and $P_{ESL\max}$ is the total power capacity of ES$_L$s. Then, as long as the lumped load power does not exceed $P_{ESL\max}$, the DC bus voltage will always be limited in the acceptable range, as endorsed by [28].

A similar merging operation can also be applied to (3), which gives the following:

$$V = V_n - n\frac{P_{ESH}}{s},\ n = (n_1^{-1} + n_2^{-2} + \cdots + n_y^{-1})^{-1}, \quad (5)$$

where n is the consolidated ID coefficient and $P_{ESH} = \sum_{i=1}^{y} P_{ESHi}$ is the total power supplied by ES$_H$s. At any point in time, the power balance in DC MG must hold, i.e., $P_{ESL} + P_{ESH} = P_{eq}$. Slightly manipulating (4) and (5), the power sharing between the ES$_L$ and ES$_H$ clusters can be derived:

$$P_{ESL} = \frac{n/m}{s + n/m} P_{eq}, \quad (6)$$

$$P_{ESH} = \frac{s}{s + n/m} P_{eq}. \quad (7)$$

From (6) and (7), it is observed that a LPF and a HPF are inherently cast to decompose P_{eq} into low-frequency and high-frequency components, respectively. Eq. (6) suggests the ES$_L$ cluster will continuously balance the equivalent load in the steady state, whereas ES$_H$s assist only to compensate the sudden change in P_{eq}. In this sense, the dynamic power allocation in the HESS has been achieved.

2) Power sharing among ES$_L$s.

Upon (6), P_{ESL} should be appropriately shared by all ES$_L$s. By virtue of (2), the relations of P_{ESLi} can be delineated as

$$P_{ESL1} : P_{ESL2} : \cdots : P_{ESLx} = m_1^{-1} : m_2^{-1} : \cdots : m_x^{-1}. \quad (8)$$

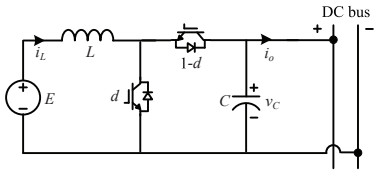

Fig. 2. A commonly used DC/DC buck-boost converter.

3) Power sharing among ES$_H$s.

Similar to (8), surging power P_{ESH} can also be distributed to ES$_H$s such that P_{ESHi} is subject to the following expression:

$$P_{ESH1} : P_{ESH2} : \cdots : P_{ESHy} = n_1^{-1} : n_2^{-1} : \cdots : n_y^{-1}. \quad (9)$$

Comparing (8) and (9) indicates that ID duplicates the power sharing characteristics in traditional V-P droops. For either V-P or ID, the powers generated by ES$_L$s or ES$_H$s can be regulated as inversely proportional to the respective droop coefficients. If m_i and n_i are properly designed, as in [2], [3], steady state power allocation in ES$_L$s and surging power distribution among ES$_H$s according to their power ratings can be favorably realized.

B. DC/DC Converter Modeling

As explained above, the implementations of V-P droop and ID inevitably requires DC/DC converters whose controllers should be carefully designed. Fig. 2 shows the topology of a widely used buck-boost converter whose average model in a switching period can be written as follows,

$$\begin{cases} \dot{i}_L = E/L - (1-d)v_C/L \\ \dot{v}_C = (1-d)i_L/C - i_o/C \end{cases}, \quad (10)$$

where $L = L_0 + \Delta_L$ and $C = C_0 + \Delta_C$ are the real inductance and capacitance. L_0 and C_0 are the nominal inductance and capacitance, respectively. Δ_L and Δ_C stand for parameter uncertainties. i_L, v_C and i_o represent the inductor current, capacitor voltage and output current. d is the duty cycle which will be compared with a modulation wave to generate drive signals for power switches. E is the input voltage that could represent either ES$_{Li}$ or ES$_{Hi}$. Compared with a buck converter for which the dynamic equations are in linear form [29], for (10), the control input (d) and state variables (i_L, v_C) are coupled together. This coupling cause difficulty in adopting conventional linear controllers to stabilizer system states, but an alternative control strategy should be studied, thus motivating the proposition of compound stabilizer design in this paper. Rearranging (10) into one in terms of L_0, C_0, Δ_L and Δ_C gives the following:

$$\begin{cases} \dot{i}_L = \dfrac{E}{L_0} - \dfrac{(1-d)v_C}{L_0} + \left[-\dfrac{E\Delta_L}{L_0 L} + \dfrac{(1-d)v_C\Delta_L}{L_0 L} \right] \\ \dot{v}_C = \dfrac{(1-d)i_L}{C_0} - \dfrac{i_o}{C_0} + \left[-\dfrac{(1-d)i_L\Delta_C}{C_0 C} + \dfrac{i_o\Delta_C}{C_0 C} \right] \end{cases}. \quad (11)$$

To better manage the differential equations in (11), as understood from [30] and [29], coordinate transformations in (12) can be performed to obtain a canonical converter model depicted as

$$z_1 = 0.5L_0 i_L^2 + 0.5C_0 v_C^2,\ z_2 = Ei_L. \quad (12)$$

Taking the time derivatives of z_1 and z_2 separately gives

$$\begin{cases} \dot{z}_1 = L_0 i_L \dot{i}_L + C_0 v_C \dot{v}_C = Ei_L + \delta_1 \\ \dot{z}_2 = E\dot{i}_L = E^2/L_0 - (1-d)Ev_c/L_0 + \delta_2 \end{cases}. \quad (13)$$

Slightly manipulating (13) yields

$$\dot{z}_1 = z_2 + \delta_1,\ \dot{z}_2 = u + \delta_2, \quad (14)$$

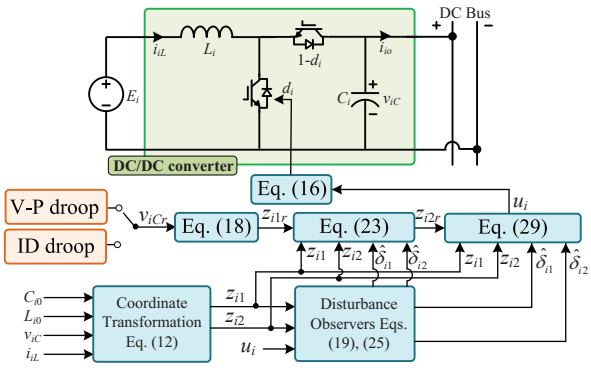

Fig. 3. Diagram of the decentralized compound stabilizer for the ith converter.

where δ_1 and δ_2 are system disturbances and u is the equivalent control input. These variables are detailed as follows:

$$\begin{cases} \delta_1 = -\dfrac{v_C i_o}{} + \dfrac{v_C i_o \Delta_C}{C} - \dfrac{E i_L \Delta_L}{L} \\ \qquad + \dfrac{(1-d) i_L v_C \Delta_L}{L} - \dfrac{(1-d) i_L v_C \Delta_C}{C} \\ \delta_2 = -\dfrac{E^2 \Delta_L}{L_0 L} + \dfrac{(1-d) E v_C \Delta_L}{L_0 L} \\ u = \dfrac{E^2}{L_0} - \dfrac{(1-d) E v_C}{L_0} \end{cases}. \tag{15}$$

According to the third expression in (15), the original duty cycle d in (10) can be written as

$$d = 1 - \frac{E}{v_C} + \frac{L_0 u}{E v_C}. \tag{16}$$

By means of the presented coordinate transformations, the overall dynamics in the DC/DC converter are extracted and embodied in (14). It is apparent that (14) is an integrator chain where each differential equation is coupled with a disturbance, which facilitates large signal stabilizer design as shown in the next section.

III. Decentralized Compound Stabilizer

To demonstrate that the decentralized compound stabilizer would uniformly cooperate with either V-P droop or ID, without loss of generality, the subscript "i" is designated to all variables in (14) to indicate that the dynamic system corresponds to the ith converter possessed by the HESS in Fig. 1, that is,

$$\begin{cases} \dot{z}_{i1} = z_{i2} + \delta_{i1} \\ \dot{z}_{i2} = u_i + \delta_{i2} \end{cases}, \tag{17}$$

Presuming that the output power of a converter equals its input power, then based on (12), the corresponding reference signal of z_{i1} can be determined provided a known voltage reference v_{iCr},

$$\begin{aligned} z_{i1r} &= 0.5 C_{i0} v_{iCr}^2 + 0.5 L_{i0} i_{iLr}^2 \\ &= 0.5 C_{i0} v_{iCr}^2 + 0.5 L_{i0} (i_{io} v_{iC} / E_i)^2. \end{aligned} \tag{18}$$

The intention is to find a correct u_i to enforce z_{i1} tracking z_{i1r} in (18). For this purpose, a recursive stabilizer design guideline is provided in this section following the standard backstepping framework documented in [31]. The guideline is divided into two stages.

Stage 1: Find a virtual control law to regulate z_{i1}.

The difference between z_{i1} and z_{i1r} is defined as the tracking error $e_{i1} = z_{i1} - z_{i1r}$. A nonlinear disturbance observer for estimating δ_{i1} can be designed below:

$$\hat{\delta}_{i1} = l_{i1}(z_{i1} - \varphi_{i1}),\ \dot{\varphi}_{i1} = z_{i2} + \hat{\delta}_{i1},\ l_{i1} > 0, \tag{19}$$

where $\hat{\delta}_{i1}$ is the observed quantity. φ_{i1} and l_{i1} are the intermediate state and tunable gain, respectively. Upon (17) and (19), the observer error, i.e., $e_{\delta_{i1}} = \delta_{i1} - \hat{\delta}_{i1}$, has the following dynamic,

$$\dot{e}_{\delta i1} = -l_{i1} e_{\delta i1} + \dot{\delta}_{i1}. \tag{20}$$

Then, a Lyapunov function incorporating both e_{i1} and $e_{\delta_{i1}}$ can be formed as

$$V_{i1} = 0.5 e_{i1}^2 + 0.5 e_{\delta i1}^2. \tag{21}$$

Taking the time derivative along its trajectory gives

$$\begin{aligned} \dot{V}_{i1} &= e_{i1}\dot{e}_{i1} + e_{\delta i1}\dot{e}_{\delta i1} \\ &= e_{i1}(z_{i2} + \delta_{i1} - \dot{z}_{i1r}) + e_{\delta i1}\dot{e}_{\delta i1} \\ &= e_{i1}(z_{i2r} + e_{i2} + \delta_{i1} - \dot{z}_{i1r}) + e_{\delta i1}\dot{e}_{\delta i1}. \end{aligned} \tag{22}$$

In (22), z_{i2r} is the virtual control law for e_{i1} regulation. It is actually the reference signal for state z_{i2} and e_{i2} denotes the tracking error such that $e_{i2} = z_{i2} - z_{i2r}$. z_{i2r} can thus be designed as

$$z_{i2r} = -k_{i1} e_{i1} - \hat{\delta}_{i1} + \dot{z}_{i1r},\ k_{i1} > 0. \tag{23}$$

Substituting (20) and (23) into (22) yields

$$\dot{V}_{i1} = -k_{i1} e_{i1}^2 - l_{i1} e_{\delta_{i1}}^2 + e_{i1} e_{i2} + e_{i1} e_{\delta_{i1}} + e_{\delta i1}\dot{\delta}_{i1}. \tag{24}$$

Stage 2: Find an equivalent control input to regulate z_{i1} and z_{i2}.

A disturbance observer similar to (19) can be adopted in the second stage to estimate the value of δ_{i2}:

$$\hat{\delta}_{i2} = l_{i2}(z_{i2} - \varphi_{i2}),\ \dot{\varphi}_{i2} = u + \hat{\delta}_{i2},\ l_{i2} > 0. \tag{25}$$

The differential equation regarding the estimation error is

$$\dot{e}_{\delta i2} = -l_{i2} e_{\delta i2} + \dot{\delta}_{i2}. \tag{26}$$

Subsequently, the second Lyapunov function including V_{i1}, e_{i2} and $e_{\delta_{i2}}$ is constructed below

$$V_{i2} = V_{i1} + 0.5 e_{i2}^2 + 0.5 e_{\delta i2}^2. \tag{27}$$

The time derivative of V_{i2} can be accordingly computed as,

$$\begin{aligned} \dot{V}_{i2} &= \dot{V}_{i1} + e_{i2}\dot{e}_{i2} + e_{\delta i2}\dot{e}_{\delta i2} \\ &= \dot{V}_{i1} + e_{i2}(u_i + \delta_{i2} - \dot{z}_{i2r}) + e_{\delta i2}\dot{e}_{\delta i2} \\ &= \dot{V}_{i1} + e_{i2}(u_i + \delta_{i2} + k_{i1}\dot{e}_{i1} + \dot{\hat{\delta}}_{i1} - \ddot{z}_{i1r}) + e_{\delta i2}\dot{e}_{\delta i2} \end{aligned} \tag{28}$$

Notice that $\dot{e}_{i1} = z_{i2} + \delta_{i1} - \dot{z}_{i1r}$. With the substitution of $\dot{e}_{i1}$ into (28), the control signal u_i can be composed as

$$u_i = -k_{i2} e_{i2} - \hat{\delta}_{i2} - k_{i1}(z_{i2} + \hat{\delta}_{i1} - \dot{z}_{i1r}) + \ddot{z}_{i1r},\ k_{i2} > 0. \tag{29}$$

Fig. 3 shows the schematic how u_i is constituted through the derivations from (18) to (28). (29), $\dot{V}_{i2}$ can be reduced to

$$\begin{aligned} \dot{V}_{i2} =& \dot{V}_{i1} - k_{i2} e_{i2}^2 - l_{i2} e_{\delta_{i2}}^2 + e_{i2} e_{\delta i2} + k_{i1} e_{i2} e_{\delta i1} + e_{\delta i2}\dot{\delta}_{i2} \\ =& -k_{i1} e_{i1}^2 - l_{i1} e_{\delta_{i1}}^2 - k_{i2} e_{i2}^2 - l_{i2} e_{\delta_{i2}}^2 + e_{i1} e_{i2} + e_{i1} e_{\delta_{i1}} \\ &+ k_{i1} e_{i2} e_{\delta i1} + e_{i2} e_{\delta i2} + e_{\delta i1}\dot{\delta}_{i1} + e_{\delta i2}\dot{\delta}_{i2} + e_{\delta i2}\dot{\hat{\delta}}_{i1}. \end{aligned} \tag{30}$$

It is worth mentioning that the terms $e_{i1}e_{i2}$, $e_{i1}e_{\delta_{i1}}$, $e_{i2}e_{\delta i1}$, $e_{i2}e_{\delta i2}$, $e_{\delta i1}\dot{\delta}_{i1}$, $e_{\delta i2}\dot{\delta}_{i2}$, $e_{\delta i2}\dot{\hat{\delta}}_{i1}$ in (30) are subjected to the subsequent formulas by using completion of squares:

$$e_{i1} e_{i2} \leqslant 0.5 e_{i1}^2 + 0.5 e_{i2}^2, \tag{31}$$

$$e_{i1} e_{\delta_{i1}} \leqslant 0.5 e_{i1}^2 + 0.5 e_{\delta_{i1}}^2, \tag{32}$$

$$e_{i2} e_{\delta i1} \leqslant 0.5 e_{i2}^2 + 0.5 e_{\delta i1}^2, \tag{33}$$

$$e_{i2} e_{\delta i2} \leqslant 0.5 e_{i2}^2 + 0.5 e_{\delta i2}^2, \tag{34}$$

$$e_{\delta i1}\dot{\delta}_{i1} \leqslant 0.5 e_{\delta i1}^2 + 0.5 \delta_{i1}^2, \tag{35}$$

$$e_{\delta i2}\dot{\delta}_{i2} \leqslant 0.5 e_{\delta i2}^2 + 0.5 \dot{\delta}_{i2}^2, \tag{36}$$

$$e_{\delta i2}\dot{\hat{\delta}}_{i1} \leqslant 0.5 e_{\delta i2}^2 + 0.5 \dot{\hat{\delta}}_{i1}^2. \tag{37}$$

Substituting the above seven inequalities into (30) gives rise to

$$\begin{aligned} \dot{V}_{i2} \leqslant& -(k_{i1} - 1) e_{i1}^2 - (l_{i1} - 1.5) e_{\delta_{i1}}^2 - (k_{i2} - 1 - 0.5 k_{i1}) e_{i2}^2 \\ &- (l_{i2} - 1 - 0.5 k_{i1}) e_{\delta_{i2}}^2 + \dot{\delta}_{i1}^2 + \dot{\delta}_{i2}^2 + \dot{\hat{\delta}}_{i1}^2. \end{aligned} \tag{38}$$

To achieve input to state stability (ISS) as stipulated in [30], for (38), the coefficients accompanying e_{i1}^2, $e_{\delta_{i1}}^2$, e_{i1}^2 and $e_{\delta_{i2}}^2$ should be positive, i.e.,

$$\begin{aligned} k_{i1}-1>0 \Rightarrow k_{i1}>1,\ l_{i1}-1.5>0 \Rightarrow l_{i1}>1.5,\\ k_{i2}-1-0.5k_{i1}>0 \Rightarrow k_{i2}>1+0.5k_{i1},\\ l_{i2}-1-0.5k_{i1}>0 \Rightarrow l_{i2}>1+0.5k_{i1}. \end{aligned} \tag{39}$$

Further considering that the disturbances appearing in (17) have physical meanings, it is reasonable to presume that the magnitudes of the disturbances and their derivatives are limited values:

$$\max(\delta_{i1}^2,\ \delta_{i2}^2,\ \dot{\delta}_{i1}^2,\ \dot{\delta}_{i2}^2) \leqslant D_i,\ D_i \in \mathbb{R}^+. \tag{40}$$

The same assumption also applies to $\dot{\hat{\delta}}_{i1}^2$, that is,

$$\max(\hat{\delta}_{i1}^2,\ D_i) \leqslant \varpi_i,\ \varpi_i \in \mathbb{R}^+. \tag{41}$$

These presumptions would fairly lay the groundwork for the system-level large signal stability analyses in the later section.

IV. System-Level Large Signal Stability Analysis

[C 2.1] **Theorem**: By applying the proposed compound stabilizer to all energy storage interfaced converters, the entire HESS will be autonomously stabilized in the large signal sense, which means the collective Lyapunov function of whole HESS has a negative derivative around any proper equilibrium.

Proof. With inequalities (40), (41) in mind and revisiting (38), $\dot{V}_{i2}$ can now be scaled as

$$\begin{aligned} \dot{V}_{i2} &\leqslant -(k_{i1}-1)e_{i1}^2-(l_{i1}-1.5)e_{\delta_{i1}}^2-(k_{i2}-1-0.5k_{i1})e_{i2}^2\\ &\quad -(l_{i2}-1-0.5k_{i1})e_{\delta_{i2}}^2+3\varpi_i\\ &\leqslant -\kappa_i(0.5e_{i1}^2+0.5e_{\delta_{i1}}^2+0.5e_{i2}^2+e_{\delta_{i2}}^2)+3\varpi_i\\ &\leqslant -\kappa_i V_{i2}+3\varpi_i, \end{aligned} \tag{42}$$

where $\kappa_i = \min\{2(k_{i1}-1),\ 2(l_{i1}-1.5),\ 2(k_{i2}-1-0.5k_{i1}),\ 2(l_{i2}-1-0.5k_{i1})\}$. Note that inequality (42) reveals error behaviors in a particular power converter. To examine the stability of the entire HESS, a collective Lyapunov function encompassing the dynamics of all converters could be formulated

$$\boldsymbol{V}=\sum_{i=1}^{x+y}(0.5e_{i1}^2+0.5e_{\delta_{i1}}^2+0.5e_{i2}^2+0.5e_{\delta_{i2}}^2)=\sum_{i=1}^{x+y}V_{i2}. \tag{43}$$

Differentiation on (43) leads to

$$\begin{aligned} \dot{\boldsymbol{V}}&=\sum_{i=1}^{x+y}\dot{V}_{i2}\leqslant\sum_{i=1}^{x+y}(-\kappa_i V_{i2}+3\varpi_i)\\ &\leqslant -\kappa\boldsymbol{V}+\varpi, \end{aligned} \tag{44}$$

where $\kappa = (x+y)\min(\kappa_i)$ and $\varpi = 3(x+y)\varpi_i$. Regarding the expression of $\dot{\boldsymbol{V}}$ in (44), a column error vector $\boldsymbol{e} = [e_{11},\ e_{\delta 11},\ e_{12}, e_{\delta 12},\ \cdots, e_{(x+y)1},\ e_{\delta(x+y)1},\ e_{(x+y)2},\ e_{\delta(x+y)2}]$ can be defined, and a set with $4(x+y)$ dimensions is also be formed as $\boldsymbol{\Omega} = \{\boldsymbol{e} \in \mathbb{R}^{4(x+y)} | \boldsymbol{V} \leqslant \varepsilon\}$, where $\varepsilon > 0$ could be arbitrarily small. Notice that ϖ is a constant that is independent of κ variations. It is possible to increase κ to be sufficiently large such that

$$\varpi \leqslant \rho\kappa\varepsilon,\ 0<\rho<1. \tag{45}$$

Afterward, for any $\boldsymbol{e} \in \Theta = \mathbb{R}^{4(x+y)} \setminus \boldsymbol{\Omega}$ and hence $\boldsymbol{V} \geqslant \varepsilon$, the following expression holds:

$$\dot{\boldsymbol{V}} \leqslant -\kappa\varepsilon+\varpi. \tag{46}$$

Substituting (45) into (46), it follows that

$$\dot{\boldsymbol{V}} \leqslant -\kappa\varepsilon+\rho\kappa\varepsilon \leqslant -(1-\rho)\kappa\varepsilon<0, \tag{47}$$

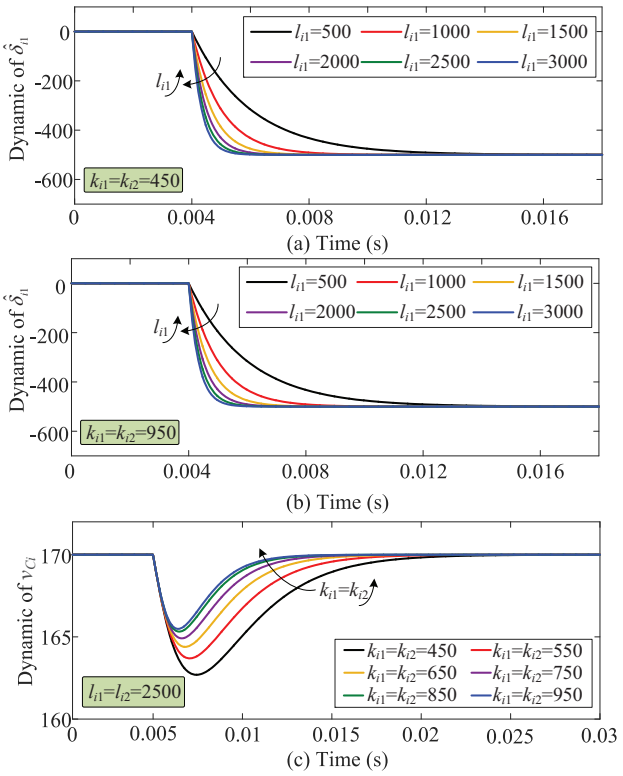

Fig. 4. [C 1.3] Parameter configuration procedures. (a) Dynamic of observer in (19) with l_{i1} being differently set when $k_{i1} = k_{i2} = 450$; (b) Dynamic of observer in (19) with l_{i1} being differently set when $k_{i1} = k_{i2} = 950$; (c) Voltage dynamic of the ith converter with k_{i1} and k_{i2} being differently set when $l_{i1} = l_{i2} = 2500$.

which means there must exist a finite time T such that any trajectory of $\boldsymbol{e}$ starting from $\boldsymbol{\Theta}$ will be captured by $\boldsymbol{\Omega}$. In this situation, it is conspicuous that the Lyapunov function (47) has a negative derivative and the whole HESS is of large signal stabilization. □

[C2.1] **Lemma**: For a given ε, by sufficiently enlarging κ, ε could be tuned infinitesimally and nearly converge to zero. Therefore, the set $\boldsymbol{\Omega}$ can be arbitrarily small and the vector $\boldsymbol{e}$ is practically regulated at the origin. Regarding the ith converter in HESS, all e_{i1}, $e_{\delta 1}$, e_{i2} and $e_{\delta 2}$ approximate to zero, indicating that $z_{i1} \to z_{i1r}$, $\hat{\delta}_{i1} \to \delta_{i1}$, $z_{i2} \to z_{i2r}$ and $\hat{\delta}_{i2} \to \delta_{i2}$. Then, the converter terminal voltage v_{iC} would closely track its reference value v_{iCr} transmitted by either V-P droop or ID.

[C2.1] **Remark**: In [2], although transient power allocation is achieved, all DC/DC converters are with double-loop PI controls, and only impedance based small signal stability is analyzed at certain steady state points. By contrast, from (17) to (47), it can be found that the proposed compound stabilizer is uniformly designed for each ES converter and implemented in a completely decentralized manner. Benefiting from the stabilizer, HESS system-level large signal stabilization can be autonomously achieved without any central controllers and communication links. This mechanism is referred to as "self-disciplined stabilization" as mentioned in the Introduction, which also exempts the modelings of RESs and CPLs from stability analyses. These features would significantly boost the efficiency of stabilizer design for real engineering applications.

V. Simulations

Following the meticulous outline of both DC/DC converter modeling and the design guideline of compound stabilizer, in this section, the key parameter configuration procedures are presented.

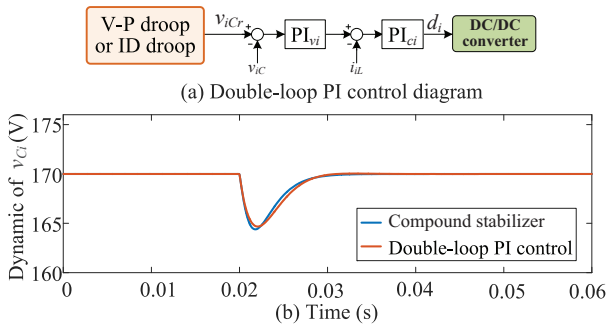

Fig. 5. [C1.3] (a) Double-loop PI control diagram; (b) Voltage dynamics of the ith DC/DC converter under the proposed compound stabilizer and the double-loop PI control, with load power surging from 0W to 400W.

Necessary comparisons of system stability margin between the compound stabilizer and conventional double-loop PI control are also provided.

A. Parameter Configuration

Although the allowable ranges of k_{i1}, k_{i2}, l_{i1} and l_{i2} were roughly stated in (39), further specifications on how these parameters are selected are highly necessary. For this purpose, the reference v_{iCr} in Fig. 3 is tentatively assigned as the system nominal voltage, i.e., 170V. Satisfying (39), the dynamic responses of observer (19) under a 500W step-up load are shown in Fig. 4(a) with l_{i1} fluctuations and $k_{i1} = k_{i2} = 450$. The converging speed of $\hat{\delta}_{i1}$ is faster when l_{i1} is increased. Specifically, the settling time of $\hat{\delta}_{i1}$ can be estimated as 8ms, 6ms, 4ms, 3ms, 2.5ms and 2ms, respectively for l_{i1} rising from 500 to 3000 in steps of 500. $\hat{\delta}_{i1}$ dynamics are further displayed in Fig. 4(b) where k_{i1} and k_{i2} are selected as 950. Comparing Fig. 4(a) and Fig. 4(b) shows that the observer dynamic has almost no relation with the backstepping controller gains, which would greatly simplify the parameter tuning process. Notice that the observer (25) for estimating δ_{i2} has the same form as (19). It can be inferred that the observer (25) would have similar dynamics to those recorded in Fig. 4(a)-(b). Hence, the dynamic profiles of $\hat{\delta}_{i2}$ are not planned here to avoid unnecessary duplications, and l_{i2} is chosen to equal l_{i1} for simplicity in this section and henceforward.

Next, parameters l_{i1} and l_{i2} in the observers remain unchanged at 2500. With a loading condition identical to that in Fig. 4(a)-(b), the voltage dynamics are plotted in Fig. 4(c). When k_{i1} and k_{i2} simultaneously increase from 450 to 950 in steps of 100, it is clear that the settling time of v_{Ci} remarkably decreases. According to the diagram of the compound stabilizer, the estimated quantities of observers would be utilized by the controller. It is thus intuitive to choose relatively large observer gains such that the observer dynamics are faster than those of backstepping controller. For instance, k_{i1}, k_{i2} can be selected as 650 and l_{i1}, l_{i2} as 2500; according to Fig. 4, the settling time of controller is estimated as 12ms, which is approximately four times longer than the observer. This set of parameters will also be employed in the subsequent comparative stability studies and hardware experiments.

B. Stability Comparison

In Sections III and IV, it has been explicated that the decentralized compound stabilizer is directly designed in time domain, and self-disciplined large signal stabilization has also been rigorously justified by Lyapunov techniques. However, for the universally used double-loop PI control in DC/DC converters, referring to the standard design guidance in [29], PI parameters are identified in the frequency domain. Then, for fair comparisons, the PI parameters can be slightly adjusted so that the dynamics of the converter terminal voltage are nearly the same under both the compound stabilizer and PI control. k_{i1}, k_{i2}, l_{i1} and l_{i2} have already been determined in the previous subsection. [C 1.2] In Fig. 5(a), double-loop PI parameters can be computed and gently adjusted based on the standard design guideline given in [29]: $k_p = 0.116$, $k_i = 426$ for the current loop and $k_p = 0.66$, $k_i = 201$ for the voltage loop. The simulation results are recorded in Fig. 5, where the ith converter works in constant voltage mode and hence the voltage reference is scheduled as the nominal value of 170V. When there is a sudden load increase of 500W at 0.02s, the voltage dip and transient duration under the proposed stabilizer and PI control are almost identical, i.e., 5V and 12ms, respectively. Notice that, in Fig. 5, once the parameters in PI and the compound stabilizer are determined, the parameters should not be changed. When multiple converters need to be work in parallel, the voltage references should be switched from the constant 170V to the value given by droop controllers, while the voltage dynamics of DC/DC converters are not impacted at all.

Based on the above settings, a complete HESS with two DC/DC converters feeding a CPL is built up, and its architecture is shown in Fig. 6. Although the equivalent load P_{eq} expressed in (1) incorporates RES powers, CPLs and resistive loads, as proposed in [32], RESs can be emulated as constant power sources in a comparatively short time period, which helps to cast resistors at the DC bus. The resistors together with the resistive loads both impart system stabilizing effects to the HESS. To investigate the harshest scenario, only the CPL is considered here and linked to the DC bus.

Output power profiles of ES$_L$ and ES$_H$ in the case of CPL stepping up from 0kW to 2.5kW in increments of 0.5kW are offered in Fig. 7. The V-P droop coefficient m and ID coefficient n are separately designed as 0.01 and 0.01pi. The crossover frequency in LPF and HPF in (6) and (7) can hence be calculated as $n/(m \times 2\pi) = 0.5$Hz. From Fig. 7, it is conspicuous that the HESS with PI controllers is of marginal stability as CPL grows to 2kW, and the overall system is entirely destabilized when CPL is further escalated to 2.5kW (see Fig. 7(a)). By contrast, the HESS with each converter regulated by the decentralized compound stabilizer can withstand CPL over 2.5kW as indicated by Fig. 7(b). These comparisons mean that the compound stabilizer provides a wider stability margin than does PI control. In fact, as stressed earlier, the proposed stabilizer contributes to the system-level large signal stabilization, which allows for stable HESS operation at any quiescent point, as long as the equilibrium does not exceed the ranges permitted by the converter hardware.

[C 1.1] It should be noted that the instability of HESS under PI controls shown by Fig. 7(a) can be theoretically analyzed with impedance ratio criterion. Focusing on the HESS configuration in Fig. 6, the two DC/DC converters with their individual PI controllers can be respectively modeled into nonlinear state space equations (see Appendix in [2]). By linearizing the models at their equilibriums, output impedances of ES$_L$ and ES$_H$ systems can be accordingly derived as Z_L and Z_H respectively, and the small signal input impedance of CPL can be depicted as Z_{CPL}. Then the minor loop transfer function of the entire HESS can be expressed as the ratio of the total impedance of parallel connected Z_L and Z_H over Z_{CPL}, i.e., $T_M = \frac{Z_L // Z_H}{Z_{CPL}}$. As understood from [26], if T_M subjects to Nyquist stability criterion, then the HESS is stable. On these bases, it is possible to give Nyquist contours of T_M of HESS under PI controls with respect to different CPLs, as in Fig. 8. When CPL is 1.5kW, Nyquist contour is far away from the critical point $(-1, j0)$ and the system is stable. The

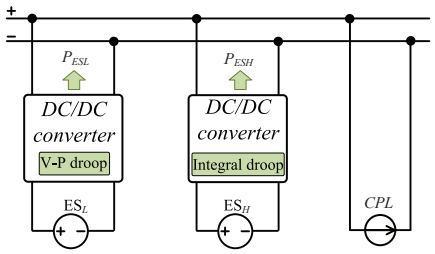

Fig. 6. HESS configuration for stability comparisons.

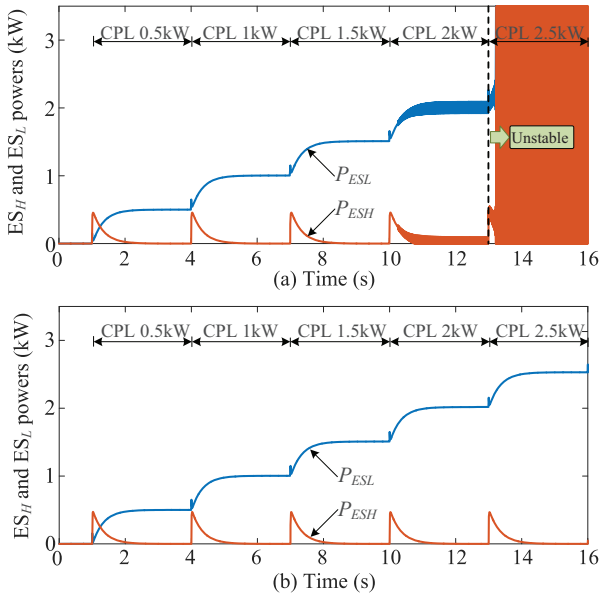

Fig. 7. Power profiles of ES_L and ES_H when the converters in Fig. 6 are with the compound stabilizer and PI control. (a) PI control; (b) Compound stabilizer.

HESS is marginally stable in the case of CPL being 2kW. The DC system is completely destabilized when CPL increases to 2.5kW, because the corresponding Nyquist contour has encircled the critical point. These observations are in perfect agreement with simulation results shown in Fig. 7.

VI. Experiments

To verify the effectiveness and feasibility of the proposed compound stabilizer, an in-house hardware experimental platform is established in Fig. 9 that includes three DC/DC converters. The converters coordinately feed a DC bus, which is loaded by a resistor and a programmable electronic load. The electronic load is simulated as a CPL whose power is consistently configured at 800W. The resistive load is 200ohm. The nominal voltage of the overall DC system is set as 170V. Detailed parameters and descriptions pertaining to the hardware platform are summarized in Table I.

A. Case 1: Two ES_Ls and one ES_H

In case 1, converters #1 and converter #2 are defined as ES_Ls, which are controlled under V-P droop schemes. The V-P droop coefficients for these two converters are identically set as 0.02. It can then be inferred that the output power of the two converters will be equalized in the steady state, and the consolidated droop coefficient can be identified as m=0.02/2=0.01 according to (4). Converter #3 is emulated as ES_H with the ID controller whose droop coefficient n is set as 0.01π. In this sense, similar to the situation in Figs. 6-7, the cutoff frequency of the naturally formed LPF/HPF is $n/(m \times 2\pi)$=0.5Hz. This suggests that components below 0.5Hz in a sudden load change will be autonomously

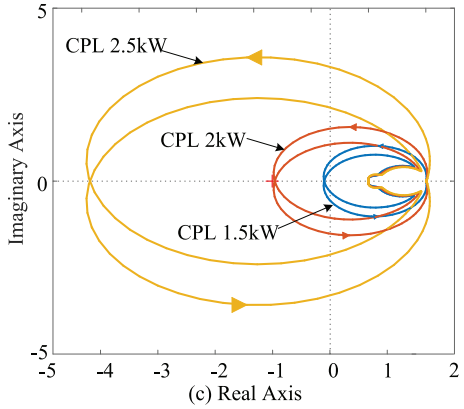

Fig. 8. [C 1.1] Nyquist contours of impedance ratio for the PI controlled HESS in Fig. 6 with different CPLs.

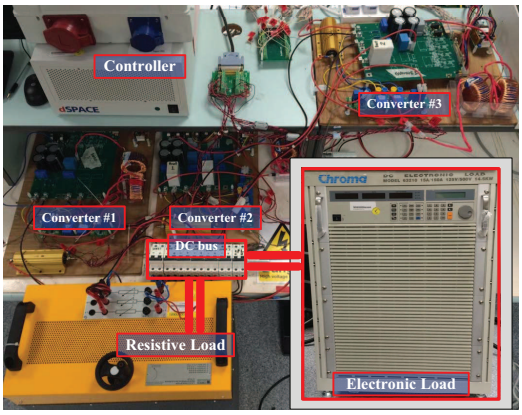

Fig. 9. Hardware experimental platform.

allocated to ES_Ls, whereas those components higher than 0.5Hz would be compensated by ES_H.

Supporting experimental results are provided in Fig. 10. In Fig. 10(a), in the beginning, only the resistive load is connected to the DC bus while the CPL is in an idle state. The power supplied by converters #1 and #2, i.e., P_{ESL1} and P_{ESL2}, is 71W, which indicates that equal power sharing in ES_Ls has been realized. Converter #3 has the power of 0W, and is ready to smooth the surging power requested by the equivalent load. When the CPL is enabled to drain a constant power of 800W from the HESS, the ES_H immediately exports power of approximately 800W to handle the high-frequency parts of the abrupt load increase. Its power slowly falls to zero in the steady state. For ES_Ls, P_{ESL1} and P_{ESL2} gradually rise to 464.5W from 71W. The equal power sharing of ES_Ls is not impaired at all, and the dynamic power allocation between ES_H and ES_Ls is also perfectly accomplished. The DC bus voltage decreases from the original 168.5V to 160.4V, and the holistic system transition requires approximately 1 second.

To demonstrate that the proper power sharing patterns stated from (4) to (9) are also tenable in the charging process, in Fig. 10(b), CPL is disabled. Instead, an additional converter controlled as the CPS is coupled to the DC bus. The CPS constantly injects 800W to the DC system regardless of bus voltage deviations. It should be mentioned that the CPS power is larger than the power required by the resistive load, and the superfluous power should be stored by the overall HESS. As visualized in Fig. 10(b), once the CPS is activated, ES_H instantly absorbs the power up to approximately 800W; the power subsequently recovers to 0W at the end of the system transition. P_{ESL}s declines to -321.7W, which implies the two ES_Ls are charged. According to these observations, it can be concluded that both transient power

TABLE I
SYSTEM PARAMETERS

Parameters	Description	Value
V_{th}	Nominal bus voltage	170 V
L_i	DC/DC converter inductance	2mH
C_i	DC/DC converter capacitance	470uF
f_{sw}	Switching frequency	10kHz
R_L	Resistive load	200ohm
CPL	Constant power load	800W
$C_{\mathrm{ES}H}$	ES_H capacity	0.213kWh
$C_{\mathrm{ES}L}$	ES_L capacity	14.4kWh

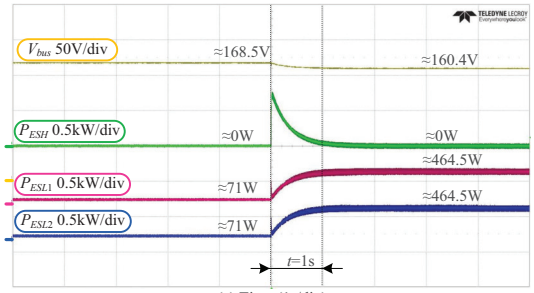

(a) Time (1s/div)

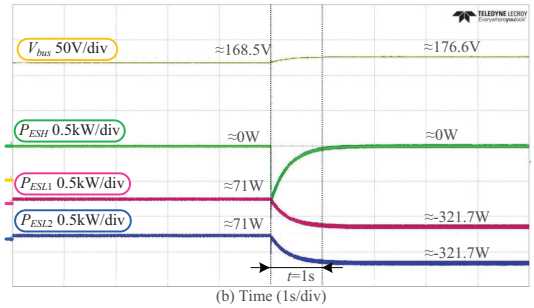

(b) Time (1s/div)

Fig. 10. Experimental results of case 1 with converters #1 and #2 working with V-P droops and converter #3 with ID ($n/m = \pi$, i.e., 0.5Hz). (a) The HESS in the discharging process; (b) The HESS in the charging process.

sharing in the entire HESS and proportional power sharing in ES_Ls are perfectly achieved.

B. Case 2: One ES_L and two ES_Ls

Unlike case 1, converters #2 and #3 are now mimicking ES_Hs, while converter #1 is acting as an ES_L. The ID coefficients for ES_Hs are individually designed as 0.02π. Afterward, referring to (5), the combined ID gain can be determined as n=0.02π/2=0.01π. The V-P droop gain is accordingly set as m=0.01 to entail that the formulated LPF and HPF have the same dynamics as in the first case. Relevant experimental results have been exhibited in Fig. 11. For the discharging mode (see Fig. 11(a)), initially, only resistive load is integrated and CPL is not configured. P_{ESH1} and P_{ESH2} are all zero, signifying that converters #2 and #3 do not provide any power to the resistor. At the instant when the CPL of 800W is executed, two ES_Hs simultaneously release power which is soon reduced to zero after system transition. The transient power is evenly shared by ES_Hs, in good agreement with the expectation of configuring the same ID droop coefficients in ES_Hs. Converter #1 singlehandedly covers the total load power in the HESS. Its output power, P_{ESL}, increases to 929W from the former value of 142W. These results suggest that the first and third types of power sharing claimed in Section II *Part A* are all attained. Comparing Fig. 10(a) and Fig. 11(a) shows that the bus voltage dynamics are almost the same. The system transition time in Fig. 11(a) can be estimated as 1s, which is also consistent with Fig. 10(a). These affinities are due to the initial system setting that the combined V-P droop coefficient and ID coefficient are equal to those in case 1.

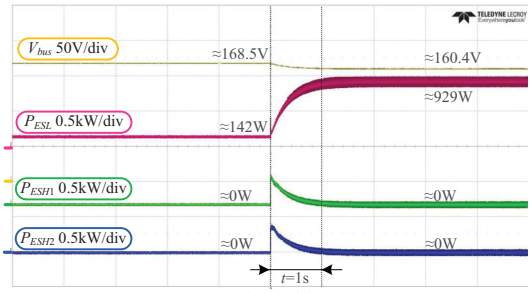

(a) Time (1s/div)

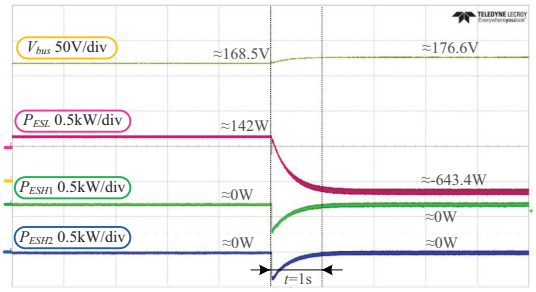

(a) Time (1s/div)

Fig. 11. Experimental results of case 2 with converter #1 working with V-P droop and converters #2 and #3 with IDs ($n/m = \pi$, i.e., 0.5Hz). (a) The HESS in the discharging process; (b) The HESS in the charging process.

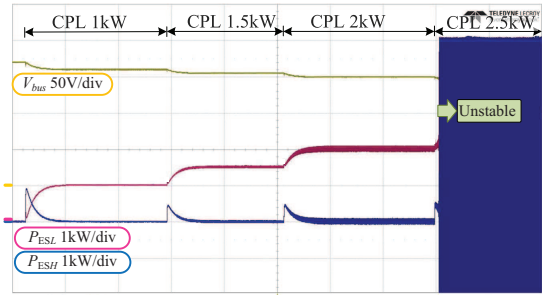

(a) Time (2s/div)

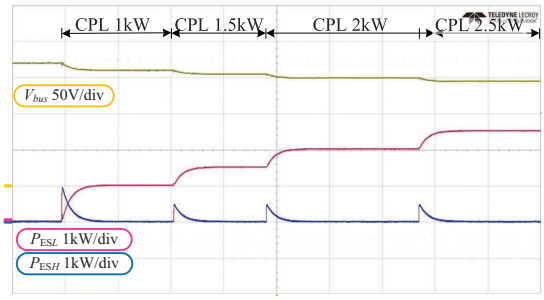

(b) Time (2s/div)

Fig. 12. Comparative stability studies for the HESS in 6 with either PI controls or compound stabilizers. (a) PI controls; (b) Compound stabilizers.

Proceeding to the charging mode in Fig. 11(b), the CPL is removed, and a CPS as in Fig. 10(b) is triggered. The ES_L power clearly reverses from 142W to -643.4W, revealing that the excess power is stored in ES_L. In the transient state, ES_Hs respond to the high-frequency components of the injected power, and ES_L tackles the low-frequency ones. Therefore, apposite transient power sharing in HESS has been favorably realized, as has power sharing between ES_Hs.

C. Case 3: Comparative stability studies

Subsequent to the simulations in Fig. 7, Fig. 12 shows the experimental results for the comparison of the HESS stability margin under both PI controls and compound stabilizers. For case 3, converters #1 and #2 are used, and only the CPLs in the previous two cases are adopted. Converter #1 stands for ES_L whereas converter #2 represents ES_H. As shown in Fig. 12(a)

that, with PI controls, the entire HESS is destabilized when the CPL increases to 2.5kW. As for the system under the proposed compound stabilizer, the HESS can tolerate the CPL up to 2.5kW, and the DC bus voltage finally falls below 150V. However, this extreme operation should not be happening in real engineering practices since large voltage drops would cause serious damages to voltage-sensitive loads. On the other hand, as in [3], it is also possible to restore the bus voltage to the nominal and to maintain transient power allocation by superposing correction signals to all droop controllers. The signals are generated by a central controller that consistently processes the difference between the real-time voltage and the nominal value, and the bus voltage can be stabilized at the nominal value in the steady state.

VII. Conclusion

This paper proposes a novel decentralized compound stabilizer for realizing system-level large signal stabilization of a HESS. In the HESS, ES_Ls and ES_Hs are respectively controlled by V-P droops and IDs. By the coordination of the two kinds of droops, the high-frequency components of load changes can be automatically compensated by ES_Hs, whereas ES_Ls supply the low-frequency ones, thereby achieving dynamic power allocations. To improve HESS stability, a self-disciplined large signal stabilization scheme is proposed in which an original compound stabilizer is well devised for each ES-interfaced converter. The stabilizer is composed of disturbance observers and a backstepping controller. The observers give the estimations of disturbances induced by parameter uncertainties and the electrical couplings of a converter system with its surroundings. The estimated quantities are subsequently offset by the controller, which ensures the converter stability in the large signal sense. As a benefit of the proposed stabilizer, the overall DC system will spontaneously achieve large signal stabilization without any communication links. Simulations show that the compound stabilizer contributes a wider stability margin than does conventional PI control. Hardware experiments verify the effectiveness and feasibility of the proposed stabilization scheme.

References

[1] G. F. Reed, "DC Technologies: Solutions to Electric Power System Advancements [Guest Editorial]," *IEEE Power and Energy Magazine*, vol. 10, no. 6, pp. 10–17, nov 2012.

[2] P. Lin, P. Wang, J. Xiao, J. Wang, C. Jin, and Y. Tang, "An Integral Droop for Transient Power Allocation and Output Impedance Shaping of Hybrid Energy Storage System in DC Microgrid," *IEEE Transactions on Power Electronics*, vol. 33, no. 7, pp. 6262–6277, jul 2018.

[3] J. Xiao, P. Wang, and L. Setyawan, "Multilevel Energy Management System for Hybridization of Energy Storages in DC Microgrids," *IEEE Transactions on Smart Grid*, vol. 7, no. 2, pp. 1–1, 2015.

[4] P. Lin, T. Zhao, B. Wang, Y. Wang, and P. Wang, "A semi-consensus strategy toward multi-functional hybrid energy storage system in dc microgrids," *IEEE Transactions on Energy Conversion*, 08 2019.

[5] Amin, R. T. Bambang, A. S. Rohman, C. J. Dronkers, R. Ortega, and A. Sasongko, "Energy Management of Fuel Cell/Battery/Supercapacitor Hybrid Power Sources Using Model Predictive Control," *IEEE Transactions on Industrial Informatics*, vol. 10, no. 4, pp. 1992–2002, nov 2014.

[6] J. Xiao, P. Wang, L. Setyawan, and Q. Xu, "Multi-Level Energy Management System for Real-Time Scheduling of DC Microgrids With Multiple Slack Terminals," *IEEE Transactions on Energy Conversion*, vol. 31, no. 1, pp. 392–400, mar 2016.

[7] B. Wang, U. Manandhar, X. Zhang, H. B. Gooi, and A. Ukil, "Deadbeat Control for Hybrid Energy Storage Systems in DC Microgrids," *IEEE Transactions on Sustainable Energy*, vol. PP, no. c, p. 1, 2018.

[8] X. Chen, M. Shi, J. Zhou, Y. Chen, W. Zuo, J. Wen, and H. He, "Distributed Cooperative Control of Multiple Hybrid Energy Storage Systems in a DC Microgrid Using Consensus Protocol," *IEEE Transactions on Industrial Electronics*, vol. PP, no. c, pp. 1–1, 2019.

[9] F. Guo, Q. Xu, C. Wen, L. Wang, and P. Wang, "Distributed Secondary Control for Power Allocation and Voltage Restoration in Islanded DC Microgrids," *IEEE Transactions on Sustainable Energy*, vol. 9, no. 4, pp. 1857–1869, oct 2018.

[10] X.-K. Liu, H. He, Y.-W. Wang, Q. Xu, and F. Guo, "Distributed Hybrid Secondary Control for a DC Microgrid via Discrete-time Interaction," *IEEE Transactions on Energy Conversion*, vol. PP, no. c, pp. 1–1, 2018.

[11] Y. Gu, W. Li, and X. He, "Frequency-coordinating virtual impedance for autonomous power management of DC microgrid," *IEEE Transactions on Power Electronics*, vol. 30, no. 4, pp. 2328–2337, 2015.

[12] H. F. Habib, C. R. Lashway, and O. A. Mohammed, "A Review of Communication Failure Impacts on Adaptive Microgrid Protection Schemes and the Use of Energy Storage as a Contingency," *IEEE Transactions on Industry Applications*, vol. 54, no. 2, pp. 1194–1207, mar 2018.

[13] X. Lu, K. Sun, J. M. Guerrero, J. C. Vasquez, L. Huang, and J. Wang, "Stability Enhancement Based on Virtual Impedance for DC Microgrids With Constant Power Loads," *IEEE Transactions on Smart Grid*, vol. 6, no. 6, pp. 2770–2783, nov 2015.

[14] L. Guo, S. Zhang, X. Li, Y. W. Li, C. Wang, and Y. Feng, "Stability Analysis and Damping Enhancement Based on Frequency-Dependent Virtual Impedance for DC Microgrids," *IEEE Journal of Emerging and Selected Topics in Power Electronics*, vol. 5, no. 1, pp. 338–350, mar 2017.

[15] M. Hamzeh, M. Ghafouri, H. Karimi, K. Sheshyekani, and J. M. Guerrero, "Power Oscillations Damping in DC Microgrids," *IEEE Transactions on Energy Conversion*, vol. 31, no. 3, pp. 970–980, 2016.

[16] M. N. Hussain, R. Mishra, and V. Agarwal, "A Frequency-Dependent Virtual Impedance for Voltage-Regulating Converters Feeding Constant Power Loads in a DC Microgrid," *IEEE Transactions on Industry Applications*, vol. 54, no. 6, pp. 5630–5639, nov 2018.

[17] S. Liu, P. Su, and L. Zhang, "A Virtual Negative Inductor Stabilizing Strategy for DC Microgrid With Constant Power Loads," *IEEE Access*, vol. 6, pp. 59 728–59 741, 2018.

[18] Y. Gu, W. Li, and X. He, "Passivity-Based Control of DC Microgrid for Self-Disciplined Stabilization," *IEEE Transactions on Power Systems*, vol. 30, no. 5, pp. 2623–2632, sep 2015.

[19] J. Yu, J. Yu, Y. Wang, Y. Cao, X. Lu, and D. Zhao, "Passivity-based active stabilization for DC microgrid applications," *CSEE Journal of Power and Energy Systems*, vol. 4, no. 1, pp. 29–38, mar 2018.

[20] M. A. Hassan, E. P. Li, X. Li, T. Li, C. Duan, and S. Chi, "Adaptive Passivity-Based Control of DC-DC Buck Power Converter with Constant Power Load in DC Microgrid Systems," *IEEE Journal of Emerging and Selected Topics in Power Electronics*, vol. PP, no. c, p. 1, 2018.

[21] P. Lin, C. Zhang, P. Wang, and J. Xiao, "A Decentralized Composite Controller for Unified Voltage Control with Global System Large-Signal Stability in DC Microgrids," *IEEE Transactions on Smart Grid*, 2018.

[22] P. Lin, C. Zhang, J. Wang, C. Jin, and P. Wang, "On autonomous large signal stabilization for islanded multi-bus dc microgrids: A uniform nonsmooth control scheme," *IEEE Transactions on Industrial Electronics*, pp. 1–1, 2019.

[23] D. Marx, P. Magne, B. Nahid-Mobarakeh, S. Pierfederici, and B. Davat, "Large Signal Stability Analysis Tools in DC Power Systems With Constant Power Loads and Variable Power Loads—A Review," *IEEE Transactions on Power Electronics*, vol. 27, no. 4, pp. 1773–1787, apr 2012.

[24] M. Kabalan, P. Singh, and D. Niebur, "Large Signal Lyapunov-Based Stability Studies in Microgrids: A Review," *IEEE Transactions on Smart Grid*, vol. 8, no. 5, pp. 2287–2295, sep 2017.

[25] J. Yang, W. H. Chen, S. Li, L. Guo, and Y. Yan, "Disturbance/Uncertainty Estimation and Attenuation Techniques in PMSM Drives - A Survey," *IEEE Transactions on Industrial Electronics*, vol. 64, no. 4, pp. 3273–3285, 2017.

[26] Q.-C. Zhong and X. Zhang, "Impedance-Sum Stability Criterion for Power Electronic Systems With Two Converters/Sources," *IEEE Access*, vol. 7, pp. 21 254–21 265, 2019.

[27] P. Wang, C. Jin, D. Zhu, Y. Tang, P. C. Loh, and F. H. Choo, "Distributed Control for Autonomous Operation of a Three-Port AC/DC/DS Hybrid Microgrid," *IEEE Transactions on Industrial Electronics*, vol. 62, no. 2, pp. 1279–1290, feb 2015.

[28] P. Lin, P. Wang, C. Jin, J. Xiao, X. Li, F. Guo, and C. Zhang, "A Distributed Power Management Strategy for Multi-Paralleled Bidirectional Interlinking Converters in Hybrid AC/DC Microgrids," *IEEE Transactions on Smart Grid*, pp. 1–1, 2019.

[29] S. Bacha, I. Munteanu, and A. I. Bratcu, *Power Electronic Converters Modeling and Control*, ser. Advanced Textbooks in Control and Signal Processing. London: Springer London, 2014.

[30] H. K. Khalil, *Nonlinear Systems*, ser. Pearson Education. Prentice Hall, 2002.

[31] J. Zhou and C. Wen, *Adaptive backstepping control of uncertain systems: Nonsmooth nonlinearities, interactions or time-variations*. Springer, 2008.

[32] T. Dragicevic, J. M. Guerrero, J. C. Vasquez, and D. Skrlec, "Supervisory Control of an Adaptive-Droop Regulated DC Microgrid With Battery Management Capability," *IEEE Transactions on Power Electronics*, vol. 29, no. 2, pp. 695–706, feb 2014.